IEEE Access
Multidisciplinary | Rapid Review | Open Access Journal

Received June 30, 2021, accepted July 19, 2021, date of publication July 26, 2021, date of current version July 30, 2021.

Digital Object Identifier 10.1109/ACCESS.2021.3099595

Quaternion-Based Two-Dimensional DOA Estimation for Coherent Underwater Sources Without Eigendecomposition

YI LOU, XINGHAO QU, YINHENG LU, (Graduate Student Member, IEEE), AND GANG QIAO, (Member, IEEE)

Acoustic Science and Technology Laboratory, Harbin Engineering University, Harbin 150001, China
Key Laboratory of Marine Information Acquisition and Security, Harbin Engineering University, Ministry of Industry and Information Technology, Harbin 150001, China
College of Underwater Acoustic Engineering, Harbin Engineering University, Harbin 150001, China

Corresponding author: Gang Qiao (qiaogang@hrbeu.edu.cn)

This work was supported in part by the Science and Technology on Underwater Information and Control Laboratory under Grant 6142218200410, in part by the National Natural Science Foundation of China under Grant U1806201, in part by the China Shipbuilding Industry Corporation No. 715 Research Institute under Grant 6142109180305, and in part by the State Administration of Science, Technology and Industry for National Defense under Grant JCKYS2019604SSJS006.

ABSTRACT For scenarios of coherent underwater sources at low signal-to-noise ratio (SNR), a novel quaternion-based DOA algorithm without eigendecomposition is proposed using a linear vector-hydrophone array. We construct four quaternion models by judiciously arranging the received data to fully utilize the statistical information of the incident signals. To avoid the high computational complexity caused by the eigenvalue decomposition (EVD), we introduce the computationally efficient propagator method (PM) to estimate the elevation angles of the observed signals. In the quaternion algebra framework, we statistically eliminate the additive noise, which makes the PM method exhibit a robust performance in low SNR. By fully exploiting the direction information embedded in the velocity components, we achieve a high-resolution two-dimensional (2-D) DOA estimation result with a linear vector-hydrophone array. The simulations demonstrate that the proposed method offers stable estimation performance compared with the existing non-quaternion schemes without the need for any pair matching between the estimated azimuth and elevation angles.

INDEX TERMS Quaternion, direction-of-arrival estimation, vector hydrophone, coherent signals, propagator method.

I. INTRODUCTION

The two-dimensional (2-D) direction-of-arrival (DOA) estimation for multiple underwater signals is an unfailing topic in array processing [1]–[5]. Vector hydrophones have played an important part in underwater signal processing because they show significant advantages in acquiring and utilizing acoustic information [2], [6]. In the past decades, many subspace-based methods (e.g., MUSIC [7] and ESPRIT [8]) have been applied in the field of vector hydrophones to estimate 2-D DOAs of underwater acoustic sources [2], [9]–[12]. In traditional algorithms, the outputs of an acoustic vector sensor (AVS) are modeled by a complex vector and then concatenated into a long vector [13]. However, the long-vector approach ignores the array's structure information and destroys AVS's vector characteristics. Therefore, the approach does not fully use the available information in the array data and limit performance. In recent years, quaternion-based subspace algorithms are proposed to maintain the vector nature of vector-hydrophone array outputs within a hypercomplex algebra framework [14]–[18]. In the field of electromagnetic vector sensors, quaternion-based algorithms have proved their performance superiority over the long-vector algorithms [19], [20]. However, quaternion-based algorithms for vector hydrophones have not been studied very extensively. Moreover, the correlated noise between vector hydrophones is also a practical issue in DOA estimation of underwater sources [21], which

The associate editor coordinating the review of this manuscript and approving it for publication was Hasan S. Mir.

will seriously degrade the performance of traditional subspace methods. Therefore, DOA algorithms based on vector hydrophones that fully consider underwater noise characteristics can attract much attention in many practical applications.

Traditional subspace methods are based on either the singular value decomposition (SVD) or the eigenvalue decomposition (EVD). However, EVD or SVD of a high-dimensional matrix is computationally intensive and time-consuming. Therefore, the algorithms that require neither EVD nor SVD but use linear operators to obtain the signal or noise subspace are proposed in the literature [22] (i.e., the propagator method (PM) and the orthonormal propagator method (OPM)). The DOAs of incident signals are then estimated in a way similar to that of MUSIC or ESPRIT [23]–[26]. OPM has stable performance at a medium or high signal-to-noise ratio (SNR) with low computational complexity, but the performance will severely degrade in low SNR [22]. Since cross-correlations of array data can eliminate the spatially independent noise [23], [27], many PM-like schemes based on cross-correlations have been proposed, e.g., the subspace-based method without eigendecomposition (SUMWE) [27] and other methods [2], [23], [28]–[31]. However, these algorithms only consider some cross-correlation information to obtain the DOA estimation results and do not make sufficient use of the array data. In [32], the authors applied the SUMWE algorithm to a uniform linear array (ULA) of vector hydrophones and proposed the V-SUMWE algorithm, which can be considered as an improved SUMWE by replacing pressure hydrophones in the array with vector hydrophones. However, the V-SUMWE algorithm still faces the following problems:

1) For alleviating the effect of additive noise, the authors only consider the cross-correlations between some sensor data.
2) The algorithm extracts the incident signals' angles from the direction information embedded in the velocity components while ignoring the arrival angle information in the spatial phase difference between adjacent sensors.

The underutilization of array data will seriously limit V-SUMWE's performance.

This paper proposes a SUMWE-type algorithm based on quaternion theory, namely augmented quaternion SUMWE (AQ-SUMWE), for DOA estimation of coherent underwater acoustic signals with a uniform linear vector-hydrophone array. Firstly, we construct four quaternion-based models by judiciously arranging the received signals. Two correlation matrices are then formed between the models, where the additive noise is statistically eliminated by using quaternion algebras. We achieve decoherence by using the correlation matrix smoothing technique [31], [33]. Subsequently, the computationally efficient PM algorithm is introduced to estimate the elevation angles of coherent sources. To obtain the azimuth angle estimates, we form the cross-correlation matrix between the received data from pressure and velocity hydrophones and use the estimated elevation angles to reconstruct the array response matrix [24]. Finally, the azimuth angles are extracted from the direction information in the velocity components. The proposed AQ-SUMWE algorithm does not need the pair-matching step of 2-D DOA parameters and has the following three contributions:

1) The quaternion model provides an elegant and compact way for dealing with the received data of vector sensors [14]. The quaternion modeling approach is fully utilized, and multiple quaternion-based models are constructed judiciously in the proposed method to obtain the statistical information of incoming signals. As a result, the proposed method exhibits a high-resolution performance.
2) In the quaternion algebra framework, we construct two noise-free correlation matrices at the statistical level to obtain the DOA angles. Consequently, the estimation results show robustness at low SNR.
3) In contrast to SUMWE-type methods, our method exploits not only cross-correlations but auto-correlations of the array data. Both the direction information inherent in velocity components and the spatial phase information between adjacent sensors are used to obtain 2-D directions of underwater sources. Fuller utilization of the array data enhances the accuracy performance for 2-D DOA estimation.

This article is arranged as follows. The necessary properties of quaternions and quaternion algebras are introduced in Section 2. Section 3 formulates mathematical models based on quaternions and proposes the novel AQ-SUMWE algorithm. Simulations are shown in Section 4. Section 5 summarizes the whole work.

In this paper, scalar quantities and vectors are represented in regular lowercase typefaces and lowercase boldface letters, respectively, and uppercase boldface letters are used to denote matrices. The notations $(\cdot)^T$, $(\cdot)^*$, $(\cdot)^H$, $(\cdot)^{-1}$, and $(\cdot)^\dagger$ represent transpose, conjugate, conjugate transpose, inverse, and pseudo inverse, respectively. diag$\{\cdot\}$ denotes the diagonal matrix; $E\{\cdot\}$ is the expectation operation; arg$(\cdot)$ is the phase operation; arccos$(\cdot)$ is the inverse cosine function; $\mathbf{0}$ denotes the zero vector or zero matrix; $\mathbf{I}_p$ denotes the p-dimensional identity matrix. $\mathbb{R}$, $\mathbb{C}^{(l)}$, and $\mathbb{H}$ represent real numbers, complex numbers with an imaginary unit of l, $l = i, j, k$, and quaternions, respectively.

II. QUATERNIONS AND QUATERNION ALGEBRA

A quaternion $q \in \mathbb{H}$ consists of one real part $q_0 \in \mathbb{R}$ and three imaginary parts $q_1, q_2, q_3 \in \mathbb{R}$, which is defined as

$$q = q_0 + q_1 i + q_2 j + q_3 k, \tag{1}$$

where the units i, j, k possess the following relations:

$$\begin{aligned} ii = jj = kk &= -1, \\ ij &= -ji = k, \\ jk &= -kj = i, \\ ki &= -ik = j. \end{aligned} \tag{2}$$

The Cayley-Dickson form of a quaternion q is expressed as

$$q = \underbrace{q_0 + q_1 i}_{b_0} + \underbrace{(q_2 + q_3 i)}_{b_1} j, \tag{3}$$

where $b_0, b_1 \in \mathbb{C}^{(i)}$ can be considered as the complex-valued real and imaginary parts of the quaternion q, denoted as $\mathcal{R}e\{q\}$ and $\mathcal{I}m\{q\}$, respectively.

Some necessary properties required for this work are listed as follows:

1) The conjugate operation of a quaternion q is denoted by

$$q^* = q_0 - q_1 i - q_2 j - q_3 k. \tag{4}$$

2) For quaternions $q1$ and $q2$, the conjugate of their product satisfies the following relation:

$$(q_1 q_2)^* = {q_2}^* {q_1}^*. \tag{5}$$

3) Quaternion multiplications are noncommutative, i.e., considering two quaternions $q1$ and $q2$, we have

$$q_1 q_2 \neq q_2 q_1. \tag{6}$$

4) The modulus of a quaternion q, denoted as $|q|$, is given by $|q| = \sqrt{qq^*} = \sqrt{q^* q} = \sqrt{q_0^2 + q_1^2 + q_2^2 + q_3^2}$. The inverse of a quaternion q is given as

$$q^{-1} = \frac{q^*}{|q|^2}. \tag{7}$$

5) For any complex number $x \in \mathbb{C}^{(i)}$, we have

$$jx = x^* j. \tag{8}$$

A matrix with quaternionic entries $\mathbf{Q} \in \mathbb{H}^{M \times N}$ can be represented as

$$\mathbf{Q} = \underbrace{\mathbf{Q}_0 + \mathbf{Q}_1 i}_{\mathbf{C_0}} + \underbrace{(\mathbf{Q}_2 + \mathbf{Q}_3 i)}_{\mathbf{C_1}} j, \tag{9}$$

where $\mathbf{Q}_n \in \mathbb{R}^{M \times N}$, $n = 0, 1, \ldots, 3$, and $\mathbf{C}_0, \mathbf{C}_1 \in (\mathbb{C}^{(i)})^{M \times N}$ can be denoted as $\mathcal{R}e\{\mathbf{Q}\}$ and $\mathcal{I}m\{\mathbf{Q}\}$, respectively.

The conjugate transposition of $\mathbf{Q}$ is defined as

$$\mathbf{Q}^H = \mathbf{Q}_0^T - \mathbf{Q}_1^T i - \mathbf{Q}_2^T j - \mathbf{Q}_3^T k, \tag{10}$$

or

$$\mathbf{Q}^H = \mathbf{C}_0^H - j\mathbf{C}_1^H. \tag{11}$$

Above, we have introduced some necessary definitions and properties of quaternions. More details can be found in [15].

III. ALGORITHM DEVELOPMENT

A. QUATERNION DATA MODEL

Consider that K far-field narrowband signals $\{s_k(t) \in \mathbb{C}^{(i)}, k = 1, 2, \ldots, K\}$ with the center frequency f_0 present in a homogeneous isotropic medium and impinge upon a ULA with M vector hydrophones. The presence of the kth source with the DOA angles $\{\phi_k, \theta_k\}$ is shown in Fig. 1, where ϕ_k denotes the elevation angle, and θ_k represents the azimuth angle. Each vector hydrophone used is equipped with three sensors, i.e., two orthogonally oriented velocity hydrophones and a pressure hydrophone which are co-located at the same point. We set the interval between adjacent vector hydrophones as a half-wavelength. The 3×1 manifold vector of a vector hydrophone about the kth source can be expressed as [34]

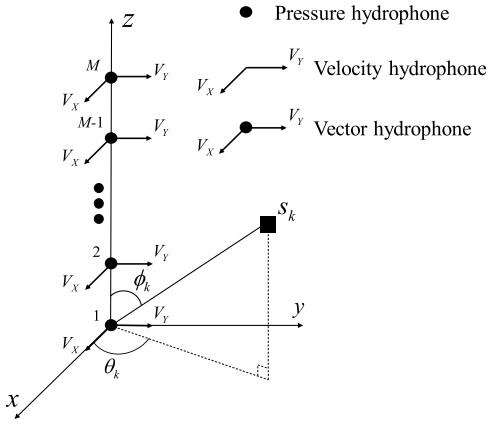

FIGURE 1. The geometrical configuration of the ULA composed of M vector hydrophones.

$$\mathbf{c}_k = \begin{bmatrix} 1 \\ u(\theta_k, \phi_k) \\ v(\theta_k, \phi_k) \end{bmatrix} = \begin{bmatrix} 1 \\ \cos\theta_k \sin\phi_k \\ \sin\theta_k \sin\phi_k \end{bmatrix}, \tag{12}$$

where u_k and v_k denote the direction cosines along the x-axis and y-axis, respectively. The first row of (12) corresponds to the pressure hydrophone, and $u(\theta_k, \phi_k)$, $v(\theta_k, \phi_k)$ in (12) correspond to the velocity hydrophones V_x, V_y in Fig. 1, respectively. Two velocity hydrophones V_x, V_y are aligned along the x-axis and y-axis, respectively.

Let the vector-hydrophone array be located along the z-axis, and the array response matrix can be given as

$$\mathbf{A}(\phi) = [\mathbf{a}(\phi_1), \mathbf{a}(\phi_2), \ldots, \mathbf{a}(\phi_K)], \tag{13}$$

where $\mathbf{a}(\phi_k) = [1, \xi_k, \ldots, \xi_k^{M-1}]^T$ is the steering vector of the kth signal. $\xi_k = e^{i2\pi d \cos\phi_k / \lambda} \in \mathbb{C}^{(i)}$ is the inter-hydrophone spatial phase factor corresponding to the kth signal, where d refers to the inter-hydrophone spacing, and λ is the signal wavelength.

Assuming a total of K fully coherent signals, the $M \times 1$ output vector with complex envelope observed by the pressure-hydrophone array at time t is expressed as

$$\mathbf{p}(t) = \sum_{k=1}^{K} \mathbf{a}(\phi_k)\, s_k(t) + \mathbf{n}_p(t) = \mathbf{A}\mathbf{s}(t) + \mathbf{n}_p(t). \tag{14}$$

Next, let $\mathbf{x}(t)$ and $\mathbf{y}(t)$ be the outputs of two subarrays constituted by the velocity hydrophones aligned along the x-axis and y-axis, respectively. $\mathbf{x}(t)$ and $\mathbf{y}(t)$ can be given by

$$\begin{aligned} \mathbf{x}(t) &= \sum_{k=1}^{K} \mathbf{a}(\phi_k)\, u(\theta_k, \phi_k) s_k(t) + \mathbf{n}_x(t) \\ &= \mathbf{A}\Gamma_x \mathbf{s}(t) + \mathbf{n}_x(t), \end{aligned} \tag{15}$$

$$\mathbf{y}(t) = \sum_{k=1}^{K} \mathbf{a}(\phi_k)\, v(\theta_k, \phi_k) s_k(t) + \mathbf{n}_y(t) = \mathbf{A}\Gamma_y \mathbf{s}(t) + \mathbf{n}_y(t), \tag{16}$$

where $\mathbf{s}(t) = [s_1(t), \ldots, s_K(t)]^T$ is the $K \times 1$ zero-mean complex signal vector, $\mathbf{n}_l(t) = [n_{l,1}(t), \ldots, n_{l,M}(t)]^T$, $l = p, x, y$ represents the $M \times 1$ additive zero-mean complex noise vector. $\Gamma_x = \mathrm{diag}\{u(\theta_1, \phi_1), \ldots, u(\theta_K, \phi_K)\}$, and $\Gamma_y = \mathrm{diag}\{v(\theta_1, \phi_1), \ldots, v(\theta_K, \phi_K)\}$.

For general scenarios, the following assumptions about the data model are valid.

1) The noise vectors $\{\mathbf{n}_p(t), \mathbf{n}_x(t), \mathbf{n}_y(t)\}$ are white Gaussian random processes in time and spatial domain and satisfy
$$E\{\mathbf{n}_{l_1}(t)\mathbf{n}_{l_2}^H(t)\} = \sigma_n^2 \mathbf{I}_K \delta_{l_1,l_2}, \quad l_1, l_2 = p, x, y, \tag{17}$$
$$E\{\mathbf{n}_{l_1}(t)\mathbf{n}_{l_2}^T(t)\} = \mathbf{0}, \quad l_1, l_2 = p, x, y, \tag{18}$$
where δ denote Kronecker delta. (18) implies that we can eliminate the additive noise by forming the pseudo-covariance matrices of noise vectors.
2) The signals $\{s_1(t), \ldots, s_K(t)\}$ are temporally white Gaussian random processes, and we have [35], [36]
$$E\{\mathbf{s}(t)\mathbf{s}^H(t)\} = \sigma_s^2 \mathbf{I}_K, \tag{19}$$
$$E\{\mathbf{s}(t)\mathbf{s}^T(t)\} = \mathbf{0}. \tag{20}$$
3) The noise vectors $\{\mathbf{n_p(t)}, \mathbf{n_x(t)}, \mathbf{n_y(t)}\}$ are independent of all signals, i.e.,
$$E\{\mathbf{s}(t)\mathbf{n}_l^H(t)\} = \mathbf{0}, \ l = p, x, y. \tag{21}$$

Next, our goal is to estimate the DOA parameters $\{\theta_k, \phi_k, k = 1, 2, \ldots, K\}$ from the observations $\mathbf{p}(t_n)$, $\mathbf{x}(t_n)$, and $\mathbf{y}(t_n)$ for $n = 1, 2, \ldots, N$, where N denotes the number of snapshots.

We introduce four quaternion-based models to better utilize the statistical information in the received signals. Four quaternion-based output vectors can be given as

$$\begin{aligned}\mathbf{u}(t) &= \mathbf{p}(t) + \mathbf{x}(t)j + \mathbf{y}(t)j \\ &= \mathbf{A}\left(\mathbf{s}(t) + \Gamma_x \mathbf{s}(t)j + \Gamma_y \mathbf{s}(t)j\right) + \mathbf{n}_1(t) \\ &= \mathbf{A}\mathbf{q}_1(t) + \mathbf{n}_1(t), \end{aligned} \tag{22}$$

$$\begin{aligned}\mathbf{v}(t) &= \mathbf{p}(t)j + \mathbf{x}(t) + \mathbf{y}(t) \\ &= \mathbf{A}\left(\mathbf{s}(t)j + \Gamma_x \mathbf{s}(t) + \Gamma_y \mathbf{s}(t)\right) + \mathbf{n}_2(t) \\ &= \mathbf{A}\mathbf{q}_2(t) + \mathbf{n}_2(t), \end{aligned} \tag{23}$$

$$\begin{aligned}\widetilde{\mathbf{u}}(t) &= \mathbf{p}^*(t) + \mathbf{x}^*(t)j + \mathbf{y}^*(t)j \\ &= \mathbf{A}^*\left(\mathbf{s}^*(t) + \Gamma_x \mathbf{s}^*(t)j + \Gamma_y \mathbf{s}^*(t)j\right) + \mathbf{n}_3(t) \\ &= \mathbf{A}^*\mathbf{q}_3(t) + \mathbf{n}_3(t), \end{aligned} \tag{24}$$

$$\begin{aligned}\widetilde{\mathbf{v}}(t) &= \mathbf{p}^*(t)j + \mathbf{x}^*(t) + \mathbf{y}^*(t) \\ &= \mathbf{A}^*\left(\mathbf{s}^*(t)j + \Gamma_x \mathbf{s}^*(t) + \Gamma_y \mathbf{s}^*(t)\right) + \mathbf{n}_4(t) \\ &= \mathbf{A}^*\mathbf{q}_4(t) + \mathbf{n}_4(t), \end{aligned} \tag{25}$$

where $\{\mathbf{n}_l(t), \ l = 1, 2, \ldots, 4\}$ are four quaternion-based noise vectors and hold the following form:

$$\begin{aligned}\mathbf{n}_1(t) &= \mathbf{n}_p(t) + \mathbf{n}_x(t)j + \mathbf{n}_y(t)j, \\ \mathbf{n}_2(t) &= \mathbf{n}_p(t)j + \mathbf{n}_x(t) + \mathbf{n}_y(t), \\ \mathbf{n}_3(t) &= \mathbf{n}_p^*(t) + \mathbf{n}_x^*(t)j + \mathbf{n}_y^*(t)j, \\ \mathbf{n}_4(t) &= \mathbf{n}_p^*(t)j + \mathbf{n}_x^*(t) + \mathbf{n}_y^*(t). \end{aligned} \tag{26}$$

B. CONSTRUCTION OF CORRELATION MATRIX

Two correlation matrices $\mathbf{R}_1$ and $\mathbf{R}_2$ between the quaternion models can be formed as

$$\begin{aligned}\mathbf{R}_1 &= E\left\{\mathbf{u}(t)\mathbf{v}^H(t)\right\} \\ &= \mathbf{A}\mathbf{R}_{q,1}\mathbf{A}^H + E\left\{\mathbf{n}_1(t)\mathbf{n}_2^H(t)\right\}, \end{aligned} \tag{27}$$

$$\begin{aligned}\mathbf{R}_2 &= E\left\{\tilde{\mathbf{u}}(t)\tilde{\mathbf{v}}^H(t)\right\} \\ &= \mathbf{A}^*\mathbf{R}_{q,2}\mathbf{A}^T + E\left\{\mathbf{n}_3(t)\mathbf{n}_4^H(t)\right\}, \end{aligned} \tag{28}$$

where $\mathbf{R}_{q,1} = E\left\{\mathbf{q}_1(t)\mathbf{q}_2^H(t)\right\}$, $\mathbf{R}_{q,2} = E\left\{\mathbf{q}_3(t)\mathbf{q}_4^H(t)\right\}$. The detailed form of $\mathbf{R}_{q,1}$ is given in (32), as shown at the bottom of the next page. Under the assumption of (20), we can derive the following relation according to (8):

$$E\{\mathbf{s}(t)j\mathbf{s}^H(t)\} = E\{\mathbf{s}(t)\mathbf{s}^T(t)\}j = \mathbf{0}. \tag{29}$$

Thus, $\mathbf{R}_{q,1}$ can be further simplified as

$$\mathbf{R}_{q,1} = \mathbf{R}_s\left(\Gamma_x + \Gamma_y\right) + \left(\Gamma_x + \Gamma_y\right)\mathbf{R}_s, \tag{30}$$

where $\mathbf{R}_s = E\{\mathbf{s}(t)\mathbf{s}^H(t)\}$ is the signal covariance matrix. Similarly, we have

$$\mathbf{R}_{q,2} = \mathbf{R}_s^*\left(\Gamma_x + \Gamma_y\right) + \left(\Gamma_x + \Gamma_y\right)\mathbf{R}_s^*. \tag{31}$$

The calculation result of $E\left\{\mathbf{n}_1(t)\mathbf{n}_2^H(t)\right\}$ is given by (34), as shown at the bottom of the next page. Consider the assumption of spatially white noise (17), the cross-correlations between noise received from different sensors should be zero. That is, for $l_1, l_2 = p, x, y$, we have

$$E\{\mathbf{n}_{l_1}(t)\mathbf{n}_{l_2}^H(t)\} = \mathbf{0}, \ l_1 \neq l_2. \tag{33}$$

On the basis of the hypothesis of (18), the following relation also holds in the quaternion algebra framework:

$$E\left\{\mathbf{n}_l(t)j\mathbf{n}_l^H(t)\right\} = E\left\{\mathbf{n}_l(t)\mathbf{n}_l^T(t)\right\}j = \mathbf{0}, \ l = p, x, y. \tag{35}$$

Note that we statistically eliminate the auto-correlation noise through the rational use of the quaternion algebraic property (8). However, V-SUMWE is powerless to eliminate the extra additive noise generated by the auto-correlations.

Based on the above derivation, the theoretical expectation of $\mathbf{n}_1(t)\mathbf{n}_2^H(t)$ should be a zero matrix. Substituting (30) into (27), we can obtain the final expression of $\mathbf{R}_1$:

$$\begin{aligned}\mathbf{R}_1 &= \mathbf{A}\big(\mathbf{R}_s\left(\Gamma_x + \Gamma_y\right) + \left(\Gamma_x + \Gamma_y\right)\mathbf{R}_s\big)\mathbf{A}^H \\ &= \mathbf{A}\Psi_1. \end{aligned} \tag{36}$$

Similarly, the final form of $\mathbf{R}_2$ can be derived as

$$\begin{aligned}\mathbf{R}_2 &= \mathbf{A}^*\left(\mathbf{R}_s^*\left(\Gamma_x + \Gamma_y\right) + \left(\Gamma_x + \Gamma_y\right)\mathbf{R}_s^*\right)\mathbf{A}^T \\ &= \mathbf{A}^*\Psi_2. \end{aligned} \tag{37}$$

Here, $\mathbf{R}_1$ and $\mathbf{R}_2$ are two noise-free matrices. Hence, the PM method based on the matrix partitioning shows a

TABLE 1. Data utilization of V-SUMWE.

$\mathbf{Z}_x\mathbf{Z}_y^H$	$\mathbf{Z}_1$	$\mathbf{Z}_2$	$\mathbf{Z}_3$	$\mathbf{Z}_4$	$\mathbf{Z}_5$
$\mathbf{Z}_1$		○	○	○	○
$\mathbf{Z}_2$	○				
$\mathbf{Z}_3$	○				
$\mathbf{Z}_4$	○				
$\mathbf{Z}_5$	○				

TABLE 2. Data utilization of AQ-SUMWE.

$q_x\widetilde{q}_y^*$	$\widetilde{q}_1$	$\widetilde{q}_2$	$\widetilde{q}_3$	$\widetilde{q}_4$	$\widetilde{q}_5$
q_1	•	•	•	•	•
q_2	•	•	•	•	•
q_3	•	•	•	•	•
q_4	•	•	•	•	•
q_5	•	•	•	•	•

stable performance even in low SNR. And we can find that $\mathbf{R}_1$ and $\mathbf{R}_2$ are two complex matrices, i.e., $\mathbf{R}_1, \mathbf{R}_2 \in \left(\mathbb{C}^{(i)}\right)^{M\times M}$. Consequently, subsequent steps can be performed in the complex number field to alleviate the computational burden. However, due to the limited number of snapshots in practice, the imaginary parts with the imaginary unit of j and k are not zero, and the information contained in them is redundant for the AQ-SUMWE algorithm. Therefore, the two imaginary parts of $\mathbf{R}_1$ and $\mathbf{R}_2$ can be discarded, thus significantly improving the proposed algorithm's data utilization. Note that the approach presented in this paper can be easily extended to full-component vector sensors.

Remark 1: From the inspection of (27) and (28), both the cross-correlations and the auto-correlations of array data are exploited to enhance the AQ-SUMWE's performance. However, only some cross-correlations are utilized in V-SUMWE. Based on a 5-element vector-hydrophone array, we compared the data utilization between the two algorithms, as shown in TABLE 1 and TABLE 2. In V-SUMWE, the output of each vector sensor is modeled by a complex vector $\mathbf{z}_l \in (\mathbb{C}^{(i)})^{3\times 1}$, $l = 1, 2, \ldots, 5$. But the AQ-SUMWE method models every outputs as multiple quaternions q_l and $\widetilde{q}_l$, $l = 1, 2, \ldots, 5$ via different mapping methods. The symbol "○" indicates that the data correlation between two sensors has been utilized, and the additive noise is eliminated by (17). The symbol "•" denotes the correlation information used, where the noise is eliminated by (17) and (18). Obviously, the AQ-SUMWE algorithm makes better use of array data and achieves significant performance improvement in the simulations compared with V-SUMWE.

Remark 2: Considering the practical application scenarios of vector hydrophones, the correlation structure of the ambient noise is a noteworthy issue [21]. If the noise field is azimuthally independent (a general assumption used widely [37], [38]), for a vertical AVS array consisting of pressure and orthogonal horizontal velocity components, the noise in different components is independent of each other. But the underwater acoustic noise in the same components will be correlated, i.e., the matrix $E\left\{\mathbf{n}_l(t)\mathbf{n}_l^H(t)\right\}, l = p, x, y$ is no longer a diagonal-noise covariance matrix. V-SUMWE can alleviate the noise correlation effect using a sparsely distributed array. However, in some practical applications with a fixed space range, one cannot significantly increase array element spacing to eliminate the effect of spatially correlated noise. In this case, the performance of V-SUMWE will be degraded. But in our method, under the assumption of (18) (a reasonable assumption [39]), the result of $E\left\{\mathbf{n}_l(t)\mathbf{n}_l^T(t)\right\}, l = p, x, y$ should still be $\mathbf{0}$. That is, the relation $E\left\{\mathbf{n}_1(t)\mathbf{n}_2^H(t)\right\} = E\left\{\mathbf{n}_3(t)\mathbf{n}_4^H(t)\right\} = \mathbf{0}$ still holds even in the scenario of correlated noise, which implies that our method has a robust performance against additive noise in our scenario. Note that the stable performance is attributed to the judicious use of the quaternion algebra.

C. CORRELATION MATRIX SMOOTHING

Considering K coherent signals, we construct a matrix $\overline{\mathbf{R}}_1$ by smoothing the correlation matrix $\mathbf{R}_1$. The matrix $\overline{\mathbf{R}}_1$ can be expressed as

$$\begin{aligned}\overline{\mathbf{R}}_1 &= [\mathbf{J}_1\mathbf{R}_1, \mathbf{J}_2\mathbf{R}_1, \ldots, \mathbf{J}_K\mathbf{R}_1] \\ &= \mathbf{A}_0\left[\Phi^0\Psi_1, \Phi^1\Psi_1, \ldots, \Phi^{K-1}\Psi_1\right] \\ &= \mathbf{A}_0\Omega_1, \end{aligned} \tag{38}$$

$$\begin{aligned}\mathbf{R}_{q,1} &= E\left\{\left(\mathbf{s}(t) + \mathbf{\Gamma}_x\mathbf{s}(t)j + \Gamma_y\mathbf{s}(t)j\right)\cdot\left(-j\mathbf{s}^H(t) + \mathbf{s}^H(t)\mathbf{\Gamma}_x + \mathbf{s}^H(t)\mathbf{\Gamma}_y\right)\right\} \\ &= E\left\{\left(-\mathbf{s}(t)j\mathbf{s}^H(t) + \mathbf{s}(t)\mathbf{s}^H(t)\mathbf{\Gamma}_x + \mathbf{s}(t)\mathbf{s}^H(t)\mathbf{\Gamma}_y\right.\right. \\ &\quad +\Gamma_x\mathbf{s}(t)\mathbf{s}^H(t) + \Gamma_x\mathbf{s}(t)j\mathbf{s}^H(t)\Gamma_x + \Gamma_x\mathbf{s}(t)j\mathbf{s}^H(t)\mathbf{\Gamma}_y \\ &\quad \left.\left. + \mathbf{\Gamma}_y\mathbf{s}(t)\mathbf{s}^H(t) + \mathbf{\Gamma}_y\mathbf{s}(t)j\mathbf{s}^H(t)\mathbf{\Gamma}_x + \mathbf{\Gamma}_y\mathbf{s}(t)j\mathbf{s}^H(t)\mathbf{\Gamma}_y\right)\right\}. \end{aligned} \tag{32}$$

$$\begin{aligned}E\left\{\mathbf{n}_1(t)\mathbf{n}_2^H(t)\right\} &= E\left\{\left(\mathbf{n}_p(t) + \mathbf{n}_x(t)j + \mathbf{n}_y(t)j\right)\cdot\left(-j\mathbf{n}_p{}^H(t) + \mathbf{n}_x{}^H(t) + \mathbf{n}_y{}^H(t)\right)\right\} \\ &= E\left\{-\mathbf{n}_p(t)j\mathbf{n}_p{}^H(t) + \mathbf{n}_p(t)\mathbf{n}_x{}^H(t) + \mathbf{n}_p(t)\mathbf{n}_y{}^H(t)\right. \\ &\quad +\mathbf{n}_x(t)\mathbf{n}_p{}^H(t) + \mathbf{n}_x(t)j\mathbf{n}_x{}^H(t) + \mathbf{n}_x(t)j\mathbf{n}_y{}^H(t) \\ &\quad \left.+\mathbf{n}_y(t)\mathbf{n}_p{}^H(t) + \mathbf{n}_y(t)j\mathbf{n}_x{}^H(t) + \mathbf{n}_y(t)j\mathbf{n}_y{}^H(t)\right\}. \end{aligned} \tag{34}$$

where $\mathbf{J}_k = \left[\mathbf{0}_{1,k} \vdots \mathbf{I}_{M-K+1} \vdots \mathbf{0}_{2,k}\right]$ is a selection matrix, where $\mathbf{0}_{1,k} \in \mathbb{R}^{(M-K+1)\times(k-1)}$ and $\mathbf{0}_{2,k} \in \mathbb{R}^{(M-K+1)\times(K-k)}$ are two zero matrices. $\mathbf{A}_0$ consists of the first $M-K+1$ rows of $\mathbf{A}$, $\Phi^k = \mathrm{diag}\left\{\xi_1^k, \xi_2^k, \ldots, \xi_K^k\right\}$, $k = 0, 1, \ldots, K-1$. And we can use $\overline{\mathbf{R}}_1$ to obtain the estimated elevation angles of the K coherent signals (see Appendix A for the proof).

Define the matrix $\mathbf{R}_2^{\downarrow}$ as

$$\mathbf{R}_2^{\downarrow} = \mathbf{J}\mathbf{R}_2 = \mathbf{A}\left(\Phi^*\right)^{M-1}\Psi_2, \tag{39}$$

where $\mathbf{J}$ is an exchange matrix (i.e., every entry on the cross-correlation line of $\mathbf{J}$ equals 1, whereas all other entries are equal to zero.) Then, the smoothed matrix $\overline{\mathbf{R}}_2^{\downarrow}$ can be expressed as follows:

$$\begin{aligned}\overline{\mathbf{R}}_2^{\downarrow} &= \left[\mathbf{J}_1\mathbf{R}_2^{\downarrow}, \ldots, \mathbf{J}_K\mathbf{R}_2^{\downarrow}\right] \\ &= \mathbf{A}_0\left[\left(\Phi^*\right)^{M-1}\Psi_2, \ldots, \left(\Phi^*\right)^{M-K}\Psi_2\right] \\ &= \mathbf{A}_0\Omega_2. \end{aligned} \tag{40}$$

For further processing, we construct an augmented correlation matrix in the following form:

$$\mathbf{R} = \left[\overline{\mathbf{R}}_1, \overline{\mathbf{R}}_2^{\downarrow}\right] = \mathbf{A}_0\Omega, \tag{41}$$

where $\Omega = [\Omega_1, \Omega_2]$.

D. ESTIMATING ELEVATION ANGLES

In this section, the propagator method is introduced to obtain the signal subspace through linear operations, and then, elevation angle estimates are obtained in a similar way to that of ESPRIT.

First, we partition $\mathbf{A}_0$ into

$$\mathbf{A}_0 = \begin{bmatrix}\mathbf{A}_1 \\ \mathbf{A}_2\end{bmatrix} \begin{matrix}\} \\ \}\end{matrix} \begin{matrix}K \\ M-2K+1,\end{matrix} \tag{42}$$

where $\mathbf{A}_1$ and $\mathbf{A}_2$ consist of the first K rows and the last $M-2K+1$ rows of $\mathbf{A}_0$, respectively. $\mathbf{A}_1$ is a full rank square matrix because of the Vandermonde structure. Therefore, $\mathbf{A}_2$ can be expressed linearly by $\mathbf{A}_1$. Define a propagator matrix $\mathbf{P}_0$, and the relationship between $\mathbf{A}_1$, $\mathbf{A}_2$, and $\mathbf{P}_0$ exists as follows [22]:

$$\mathbf{A}_2 = \mathbf{P}_0\mathbf{A}_1. \tag{43}$$

Then, it follows from (43) that

$$\mathbf{P}\mathbf{A}_1 = \begin{bmatrix}\mathbf{A}_1 \\ \mathbf{A}_2\end{bmatrix} = \mathbf{A}_0, \tag{44}$$

where $\mathbf{P} \triangleq \left[\mathbf{I}_K, \mathbf{P}_0^T\right]^T$. Since $\mathbf{A}_1$ is a full rank matrix, it is obvious that the column vectors in matrix $\mathbf{P}$ span the column space (i.e., the signal subspace) of $\mathbf{A}_0$.

Use $\mathbf{P}_a$, $\mathbf{P}_b$ to represent the first $M-K$ rows and the last $M-K$ rows of $\mathbf{P}$, respectively, and similarly, the relationship between $\mathbf{A}_a$, $\mathbf{A}_b$, and $\mathbf{A}$ is also defined in the above manner. According to (44), we can obtain

$$\begin{bmatrix}\mathbf{P}_a \\ \mathbf{P}_b\end{bmatrix}\mathbf{A}_1 = \begin{bmatrix}\mathbf{A}_a \\ \mathbf{A}_b\end{bmatrix} = \begin{bmatrix}\mathbf{A}_a \\ \mathbf{A}_a\Phi\end{bmatrix}. \tag{45}$$

The matrices $\mathbf{P}_a$, $\mathbf{P}_b$, and Φ are related as

$$\mathbf{P}_a^{\dagger}\mathbf{P}_b = \mathbf{A}_1\Phi\mathbf{A}_1^{-1}, \tag{46}$$

where $\mathbf{P}_a^{\dagger} = \left(\mathbf{P}_a^H\mathbf{P}_a\right)^{-1}\mathbf{P}_a^H$. Based on (46), $\mathbf{P}_a^{\dagger}\mathbf{P}_b$ and Φ are similar matrices. Hence, we can perform EVD on $\mathbf{P}_a^{\dagger}\mathbf{P}_b$ to obtain the diagonal elements of Φ, i.e., $\{\xi_k, k = 1, 2, \ldots, K\}$. Finally, the elevation angle estimation results ϕ_k can be obtained from

$$\phi_k = \arccos\left(\frac{\arg\left(\xi_k\right)}{2\pi d/\lambda}\right), \quad k = 1, 2, \ldots, K. \tag{47}$$

Here, we estimate the elevation angle ϕ_k from the inter-sensor spatial phase factor ξ_k, which is not available in the V-SUMWE algorithm. Therefore, our approach makes fuller use of the spatial phase information.

We partition $\mathbf{R}$ into the following form to estimate the propagator:

$$\mathbf{R} = \begin{bmatrix}\mathbf{R}_a \\ \mathbf{R}_b\end{bmatrix} = \mathbf{A}_0\Omega = \begin{bmatrix}\mathbf{A}_1 \\ \mathbf{A}_2\end{bmatrix}\Omega = \begin{bmatrix}\mathbf{A}_1 \\ \mathbf{P}_0\mathbf{A}_1\end{bmatrix}\Omega, \tag{48}$$

where $\mathbf{R}_a$ and $\mathbf{R}_b$ denote the first K and the last $M-2K+1$ rows of $\mathbf{R}$, respectively. From (48), we have

$$\mathbf{R}_b = \mathbf{P}_0\mathbf{R}_a. \tag{49}$$

Hence, the propagator can be found from $\mathbf{R}_a$ and $\mathbf{R}_b$ as

$$\mathbf{P}_0 = \mathbf{R}_b\mathbf{R}_a^{\dagger} = \mathbf{R}_b\mathbf{R}_a^H\left(\mathbf{R}_a\mathbf{R}_a^H\right)^{-1}. \tag{50}$$

Assuming that we have estimated the propagator $\hat{\mathbf{P}}_0$ from the sample data, the elevation angles $\hat{\phi}_k, k = 1, 2, \ldots, K$ can be extracted from the K eigenvalues $\{\hat{\xi}_k, k = 1, 2, \ldots, K\}$ of $\hat{\mathbf{P}}_a^{\dagger}\hat{\mathbf{P}}_b$:

$$\hat{\phi}_k = \arccos\left(\frac{\arg(\hat{\xi}_k)}{2\pi d/\lambda}\right), \quad k = 1, 2, \ldots, K. \tag{51}$$

In the presence of noise, we can still perform the partition $\mathbf{R} = \left[\mathbf{R}_a^T \vdots \mathbf{R}_b^T\right]^T$. But the relation (49) no longer holds [22]. Therefore, the noise in $\mathbf{R}$ will reduce the estimation accuracy of the propagator $\mathbf{P}_0$ obtained by (50). However, in the AQ-SUMWE algorithm, the additive noise in $\mathbf{R}$ is statistically eliminated by making rational use of the properties of quaternion algebra. Hence, a more accurate propagator estimation result can be obtained in our approach than in the noisy case.

E. ESTIMATING AZIMUTH ANGLES

In this subsection, we obtain the azimuth angle estimates by using the direction information embedded in the velocity components. The cross-correlation matrix $\mathbf{R}'$ is formed between the received data from pressure and velocity hydrophones.

First, an array output vector $\mathbf{z}(t)$ can be formed by concatenating $\mathbf{x}(t)$ and $\mathbf{y}(t)$ given in (15) (16):

$$\mathbf{z}(t) = \begin{bmatrix}\mathbf{x}(t) \\ \mathbf{y}(t)\end{bmatrix}. \tag{52}$$

Subsequently, a $2M \times M$ cross-correlation matrix $\mathbf{R}'$ can be estimated as:

$$\begin{aligned}\mathbf{R}' &= E\left\{\mathbf{z}(t)\mathbf{p}^H(t)\right\} \\ &= E\left\{\begin{bmatrix}\mathbf{A}\Gamma_x\mathbf{s}(t)\\ \mathbf{A}\Gamma_y\mathbf{s}(t)\end{bmatrix}\mathbf{s}^H(t)\mathbf{A}^H\right\} + E\left\{\begin{bmatrix}\mathbf{n}_x(t)\\ \mathbf{n}_y(t)\end{bmatrix}\mathbf{n}_p^H(t)\right\} \\ &= \begin{bmatrix}\mathbf{A}\Gamma_x\mathbf{R}_s\mathbf{A}^H\\ \mathbf{A}\Gamma_y\mathbf{R}_s\mathbf{A}^H\end{bmatrix}. \end{aligned} \tag{53}$$

Note that $\left[\mathbf{n}_x^T(t)\vdots\mathbf{n}_y^T(t)\right]^T$ and $\mathbf{n}_p(t)$ are spatially independent of each other, i.e., $E\left\{\left[\mathbf{n}_x^T(t)\vdots\mathbf{n}_y^T(t)\right]^T\mathbf{n}_p^H(t)\right\} = \mathbf{0}$. Hence, the noise in $\mathbf{R}'$ has been eliminated statistically. We denote the first M rows and the last M rows of $\mathbf{R}'$ by $\mathbf{R}'_{(1:M,:)}$ and $\mathbf{R}'_{(M+1:2M,:)}$. Substituting $\mathbf{R}' = \left[\mathbf{R}'^T_{(1:M,:)}\vdots\mathbf{R}'^T_{(M+1:2M,:)}\right]^T$ into (53) yields

$$\begin{aligned}\mathbf{A}^\dagger\mathbf{R}'_{(1:M,:)} &= \Gamma_x\mathbf{R}_s\mathbf{A}^H = \mathbf{W}_x, \\ \mathbf{A}^\dagger\mathbf{R}'_{(M+1:2M,:)} &= \Gamma_y\mathbf{R}_s\mathbf{A}^H = \mathbf{W}_y. \end{aligned} \tag{54}$$

Let $\mathbf{w}_{x,k}$ and $\mathbf{w}_{y,k}$, $k = 1, 2, \ldots, K$ signify the kth rows of $\mathbf{W}_x$ and $\mathbf{W}_y$, respectively. Consider that the Γ_x and Γ_y contain the direction information provided by the particle-velocity components, i.e., the kth diagonal elements of Γ_x and Γ_y correspond to the kth signal's direction cosines $\{u_k, v_k\}$, respectively. Based on the relation $u_k \tan\theta_k = v_k$, we can establish the relationship between $\mathbf{w}_{x,k}$ and $\mathbf{w}_{y,k}$ as follows:

$$\tan\theta_k\ \mathbf{w}_{x,k} = \mathbf{w}_{y,k}. \tag{55}$$

To estimate the array response matrix $\mathbf{A}$, we can refer to (13) and use the estimated elevation angles in (51) to reconstruct $\mathbf{A}$, i.e., $\hat{\mathbf{A}} = \left[\mathbf{a}(\hat{\phi}_1), \ldots, \mathbf{a}(\hat{\phi}_K)\right]$. Therefore, the estimates of $\mathbf{W}_x$ and $\mathbf{W}_y$ can be obtained by

$$\begin{aligned}\hat{\mathbf{W}}_x &= \hat{\mathbf{A}}^\dagger\hat{\mathbf{R}}'_{(1:M,:)}, \\ \hat{\mathbf{W}}_y &= \hat{\mathbf{A}}^\dagger\hat{\mathbf{R}}'_{(M+1:2M,:)}. \end{aligned} \tag{56}$$

Then, following from (55) and (56), the kth signal's azimuth angle can be estimated as

$$\hat{\theta}_k = \arctan\left(\hat{\mathbf{w}}_{y,k}\hat{\mathbf{w}}_{x,k}^\dagger\right), \quad k = 1, 2, \ldots, K. \tag{57}$$

Note that the elevation angles estimated from (51) are automatically matched with the azimuth angles obtained from (57) in our method (see Appendix B for the proof).

Remark 3: This paper constructs two correlation matrices $\mathbf{R}$ and $\mathbf{R}'$ to obtain the 2-D directions of the coherent underwater acoustic signals. In more detail, the correlation matrix introduced in (41) exploits the spatial phase information between adjacent array elements. The correlation matrix formed in (53) utilizes the direction information inherent in the velocity components. Furthermore, the additive noise is statistically eliminated in both correlation matrices.

Remark 4: The AQ-SUMWE method reduces the computational complexity in three ways. (1) When estimating the elevation angles, we use the computationally efficient PM method instead of the EVD that is computationally intensive and time-consuming. (2) An ESPRIT-like method is used to achieve the DOA estimation after obtaining signal subspace, thus avoiding the heavy computational burden caused by searching a multidimensional spectrum in the SUMWE algorithm. (3) The correlation matrices $\mathbf{R}_1$ and $\mathbf{R}_2$ between different quaternion models should be complex matrices. Therefore, after estimating the matrices $\mathbf{R}_1$ and $\mathbf{R}_2$, we can perform subsequent steps in the complex number field to alleviate the computational burden.

F. IMPLEMENTATION OF THE AQ-SUMWE ALGORITHM

Based on the above analysis, assuming that N snapshots of received data $\{\mathbf{p}(t_n), \mathbf{x}(t_n), \mathbf{y}(t_n), n = 1, \ldots, N\}$ are available, we summarize the AQ-SUMWE algorithm as follows:

1) According to (22), (23), (24) and (25), construct four quaternion-based array output vectors $\mathbf{u}(t)$, $\mathbf{v}(t)$, $\widetilde{\mathbf{u}}(t)$ and $\widetilde{\mathbf{v}}(t)$, $n = 1, 2, \ldots, N$.
2) Estimate the correlation matrices $\mathbf{R}_1$ and $\mathbf{R}_2$ as
$$\begin{aligned}\hat{\mathbf{R}}_1 &= \mathcal{R}e\left\{\frac{1}{N}\sum_{n=1}^{N}\mathbf{u}(t_n)\mathbf{v}^H(t_n)\right\}, \\ \hat{\mathbf{R}}_2 &= \mathcal{R}e\left\{\frac{1}{N}\sum_{n=1}^{N}\tilde{\mathbf{u}}(t_n)\tilde{\mathbf{v}}^H(t_n)\right\}. \end{aligned} \tag{58}$$
3) Perform the correlation matrix smoothing following (38), (39), and (40), then construct the matrix $\mathbf{R}$ as
$$\hat{\mathbf{R}} = \left[\hat{\bar{\mathbf{R}}}_1, \hat{\bar{\mathbf{R}}}_2^{\downarrow}\right]. \tag{59}$$
4) Estimate the propagator $\mathbf{P}_0$ using (50), then, based on (46) and (51), obtain the elevation angles of incident signals.
5) Estimate the cross-correlation matrix $\mathbf{R}'$ as
$$\hat{\mathbf{R}}' = \frac{1}{N}\sum_{n=1}^{N}\mathbf{z}(t_n)\mathbf{p}^H(t_n). \tag{60}$$
6) Use the estimated elevation angles to reconstruct the array response matrix $\mathbf{A}$, then, according to (56) and (57), estimate the azimuth angles of incident signals.

G. COMPUTATIONAL COMPLEXITY ANALYSIS

The AQ-SUMWE algorithm needs four major steps: (1) Compute the correlation matrices $\hat{\mathbf{R}}_1$ and $\hat{\mathbf{R}}_2$ via (58). (2) Estimate the propagator $\mathbf{P}_0$ as $\hat{\mathbf{P}}_0 = \hat{\mathbf{R}}_b\hat{\mathbf{R}}_a^\dagger$. (3) Calculate the cross-correlation matrix $\hat{\mathbf{R}}'$ using (60). (4) Obtain $\hat{\mathbf{W}}_x$ and $\hat{\mathbf{W}}_y$ by (56). In the next derivation, a flop is defined as a floating-point addition or multiplication operation.

First, mapping data from the real number field to the quaternion field needs $2MN$ flops, where N is the number of snapshots. Because of the conjugation relation between $\hat{\mathbf{R}}_1$ and $\hat{\mathbf{R}}_2$, estimating the two matrices requires approximately $32M^2N$ flops. When calculating the correlation matrix $\hat{\mathbf{R}}'$ in (53), the number of flops needed is approximately $16M^2N$.

TABLE 3. Complexity comparison of the three algorithms.

Algorithm	Complexity
V-SUMWE	$288(M-1)N+(312M-320K)K^2$
AQ-SUMWE	$48M^2N+2MN+16M^2(K^2+K)$
FBSS-ESPRIT	$72M^2N+\mathcal{O}(27(M-K+1)^3)$

The computation of $\hat{\mathbf{P}}_0$ in (50) takes about $16K^2M(M-2K+1)+16K^3M+8K^2(M-2K+1)+\mathcal{O}(K^3)$ flops, and the calculation of $\hat{\mathbf{W}}_x$ and $\hat{\mathbf{W}}_y$ in (56) requires roughly $16M^2K+32K^2M+\mathcal{O}(K^3)$ flops, where the computational complexity required for the inversion of a $K\times K$ Hermitian matrix is $\mathcal{O}(K^3)$ [27]. Accordingly, the total number of flops required in the proposed scheme is nearly $48M^2N+2MN+16M^2(K^2+K)$ when $N\gg M\gg K$.

The approximate computational complexity of AQ-SUMWE, V-SUMWE [32], and the forward-backward spatial smoothing ESPRIT (FBSS-ESPRIT [8], [40]) algorithm is given in TABLE 3. The proposed approach requires more flops than the V-SUMWE method in return for a significant improvement of the estimation performance, as shown in the simulation part. Compared with the FBSS-ESPRIT method, the simulations demonstrate that our approach has advantages in both estimation performance and computational complexity.

IV. SIMULATIONS

By comparing with V-SUMWE [32], FBSS-ESPRIT [8], [40], and other ESPRIT-type algorithms based on AVS arrays [2], [24], we now test the performance of AQ-SUMWE. In the FBSS-ESPRIT algorithm, the azimuth angles are estimated in a similar way as [20]. For AQ-SUMWE and V-SUMWE, We apply a 12-element ULA composed of three-component vector hydrophones. Because the methods in [2], [24] employ four-component vector hydrophones to form arrays, we set the number of array elements as 9 to ensure that the hardware costs of the algorithms are comparable. For the L-shaped array-based approach in [2], we consider an array geometry with two ULAs in the $x-z$ plane, where each ULA has 5 vector sensors. For the method in [24], a 9-element uniform linear AVS array placed along the z-axis is used. Because the V-SUMWE method can improve the estimation performance by increasing the array element spacing, the estimated results with the inter-sensor spacings of half and triple wavelengths are given in the simulations. In the other algorithms, the inter-sensor spacing is set to a half wavelength. For simplicity, we assume that all signals are of equal power σ_s^2, and the SNR is defined as $10\log_{10}\left(\sigma_s^2/\sigma_n^2\right)$, where σ_n^2 denotes the power of noise.

A. ANGULAR RESOLUTION PERFORMANCE COMPARISON

In this subsection, we consider the scenarios in which two closely spaced coherent underwater signals impinge upon the array at low SNR (SNR = 3 dB) to verify the resolution performance of our method. In the simulations, two signals

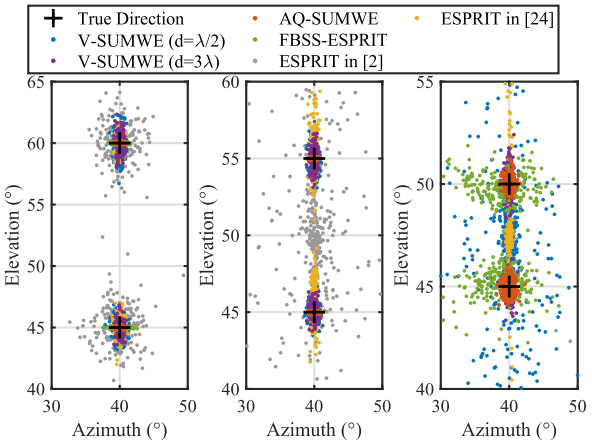

(a) $\phi_1=45°$, ϕ_2 is set to $60°, 55°, 50°$.

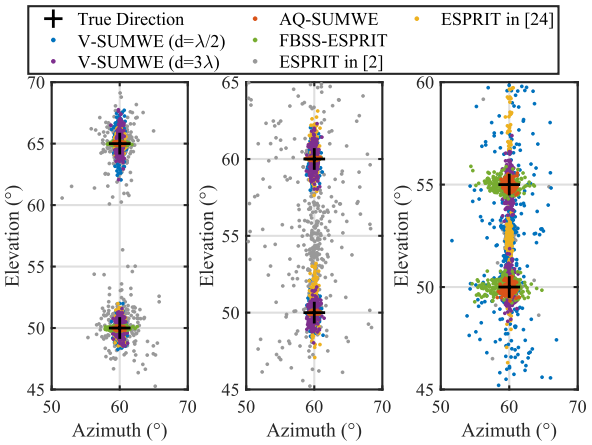

(b) $\phi_1=50°$, ϕ_2 is set to $65°, 60°, 55°$.

FIGURE 2. Angular resolution comparison in low SNR (SNR = 3 dB). The snapshot number $N=1000$. Two narrowband coherent signals impinge on the array with the azimuth angles $\theta_1=\theta_2=40°$ in Fig. 2(a), and $\theta_1=\theta_2=60°$ in Fig. 2(b).

with varying elevation angles share the same azimuth angle. Every figure in Figs. 2(a) and 2(b) displays 200 estimation results and proves the effectiveness and feasibility of the AQ-SUMWE algorithm. Obviously, AQ-SUMWE exhibits better estimation performance. Both estimation results of our method are concentrated in the true direction even with a small angle interval in low SNR.

B. ESTIMATION ACCURACY EVALUATION

In this subsection, we test the estimation accuracy of the algorithms versus different parameters. The performance metric used is the root-mean-square error (RMSE), defined as

$$\mathrm{RMSE}=\sqrt{\frac{1}{M}\sum_{m=1}^{M}\left\{\left(\hat{\theta}_{k,m}-\theta_k\right)^2+\left(\hat{\phi}_{k,m}-\phi_k\right)^2\right\}} \quad (61)$$

where K is the number of observed signals, M denotes the number of Monte Carlo trials, which is set to 5000 in the following experiments. $\hat{\theta}_{k,m}$ and $\hat{\phi}_{k,m}$ are the estimation results of θ_k and ϕ_k for the mth Monte Carlo trial, respectively. In the following simulations, we assume that two coherent

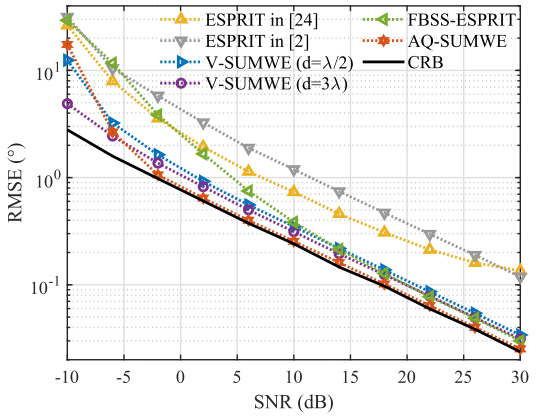

(a) Source with DOA parameters $\{\theta_1, \phi_1\} = \{20°, 30°\}$

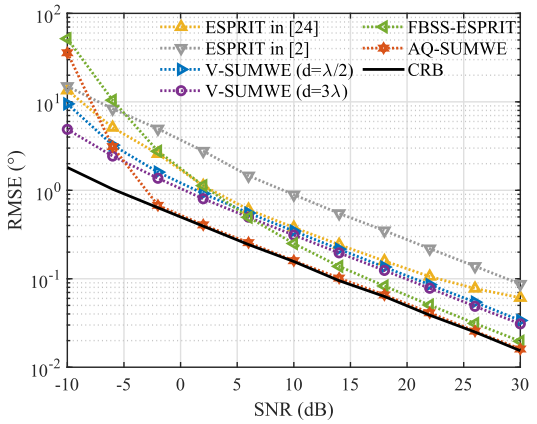

(b) Source with DOA parameters $\{\theta_2, \phi_2\} = \{60°, 50°\}$

FIGURE 3. RMSEs of the three algorithms versus SNRs. The number of snapshots is fixed at 1000. The SNRs corresponding to adjacent points in Fig. 3 differ by 4 dB, and the SNR varies from −10 dB to 30 dB.

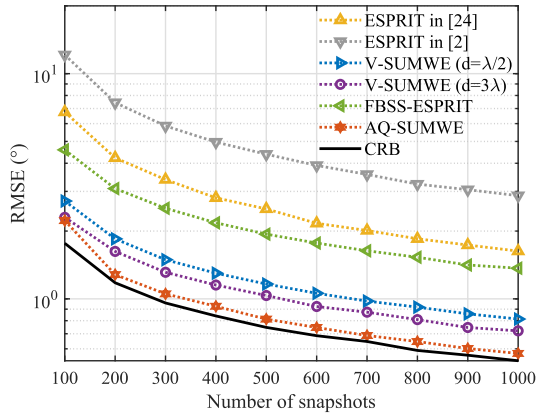

(a) Source with DOA parameters $\{\theta_1, \phi_1\} = \{20°, 30°\}$

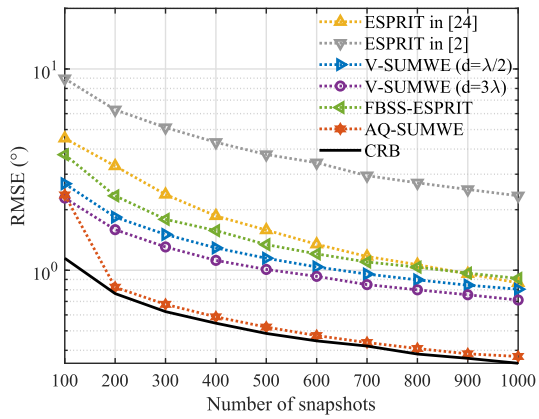

(b) Source with DOA parameters $\{\theta_2, \phi_2\} = \{60°, 50°\}$

FIGURE 4. RMSEs of the three algorithms at different snapshot numbers. SNR = 3 dB, and the snapshot number varies from 100 to 1000 with a number interval of 100.

sources are located at $\{\theta_1, \phi_1, \theta_2, \phi_2\} = \{20°, 30°, 60°, 50°\}$ in Figs. 3 and 4, and $\{\theta_1, \phi_1, \theta_2, \phi_2\} = \{30°, 40°, 40°, 60°\}$ in Fig. 5. The estimation results for each source will be given separately in different figures. CRB in [39] is used as a performance benchmark in the next simulations.

Figs. 3 and 4 plot the RMSEs of three algorithms versus SNRs and snapshot numbers, respectively. The snapshot number equals 1000 in Fig. 3, and the SNR is set to 3 dB in Fig. 4. The simulation results in these figures indicate that AQ-SUMWE performs better than other schemes in terms of estimation precision. Compared with V-SUMWE, the improvement of performance can be explained as a fuller utilization of the array data. In Fig. 5, we investigate the estimation performance of AQ-SUMWE versus the number of array elements. In this experiment, the number of snapshots is set to 1000, and the SNR is 3 dB. From Fig. 5, one can observe that AQ-SUMWE can still offer performance superior to V-SUMWE.

C. PERFORMANCE VERSUS CORRELATED NOISE

In Fig. 6, the effect of correlated noise on the algorithm performance is explored. According to [21], we assume that the noise in the different components of vector hydrophones is independent of each other. And the mathematical models of the received noise vectors by different components are expressed as

$$\mathbf{n}_l(t) = \sqrt{\rho} n_{l,0}(t)\mathbf{1}_M + \sqrt{1-\rho}\mathbf{n}'_l(t), \quad l = p, x, y \quad (62)$$

where $\mathbf{n}'_l(t) = \left[n_{l,1}(t), n_{l,2}(t), \ldots, n_{l,M}(t)\right]$, and $\mathbf{1}$ denotes an all-one $M \times 1$ row vector. $n_{l,0}(t), n_1(t), n_2(t), \ldots, n_M(t)$ are independent of each other and with equal power. The correlation factor ρ is varied between 0 and 1, which measures the noise correlation across the sensors.

When the element spacing d is set as triple wavelength, the correlation of the noise between different sensors has been ignored [21], and the performance of V-SUMWE ($d = 3\lambda$) can be used as a performance reference in the simulation. In Fig. 6, as the correlation factor ρ increases, the performance of FBSS-ESPRIT and V-SUMWE ($d = 0.5\lambda$) will significantly degrade. However, thanks to the quaternion algebra framework, the proposed AQ-SUMWE algorithm shows robustness to spatially correlated noise and provides more accurate DOA estimates compared with other methods.

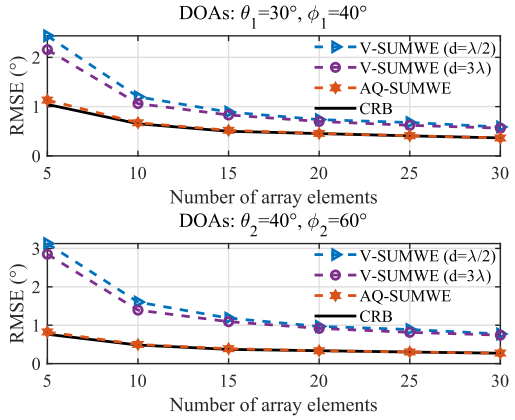

FIGURE 5. RMSEs of the three algorithms versus the number of array elements, where the number of array elements is increased from 5 to 30 with an interval of 5.

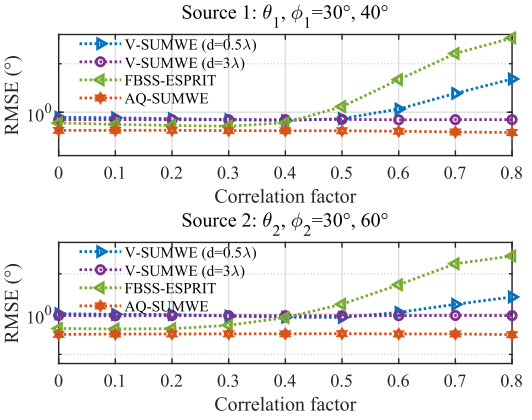

FIGURE 6. RMSEs versus the correlation factor ρ, where SNR = 3 dB, the number of snapshots $L = 1000$.

V. CONCLUSION

A novel quaternion-based DOA estimation algorithm called AQ-SUMWE has been proposed. We integrate multiple signal models based on quaternion frameworks to fully utilize the array data. And the additive noise is statistically eliminated by rational use of the quaternion algebra properties. As a result, the computationally efficient PM method offers performance superiority in elevation angle estimation. By exploiting the spatial phase difference between adjacent sensors and the directional information embedded in the velocity components, we achieve high-resolution 2-D DOA estimation for coherent underwater sources. Simulation results demonstrate that the fuller data utilization and noise elimination provide stable estimation performance for the proposed algorithm.

APPENDIX A

We now prove that the matrix $\overline{\mathbf{R}}_1$ in (38) can be used to estimate the DOAs of K coherent signals. We have known that $\overline{\mathbf{R}}_1 = \mathbf{A}_0\Omega_1$, where

$$\Omega_1 = \left[\mathbf{I}_K, \Phi^1, \ldots, \Phi^{K-1}\right]\Psi_1. \tag{63}$$

Denote the mth column of Ψ_1 as $\boldsymbol{\psi}_{1,m}$, and let

$$\Omega_{1,m} = \left[\mathbf{I}_K, \Phi^1, \ldots, \Phi^{K-1}\right]\boldsymbol{\psi}_{1,m}. \tag{64}$$

Naturally, we have

$$\overline{\mathbf{R}}_1 = \left[\overline{\mathbf{R}}_{1,1}, \ldots, \overline{\mathbf{R}}_{1,M}\right] = \mathbf{A}_0\left[\Omega_{1,1}, \ldots, \Omega_{1,M}\right]. \tag{65}$$

Considering that $\boldsymbol{\psi}_{1,m} = \left[\psi_{1,m,1}, \psi_{1,m,2}, \ldots, \psi_{1,m,K}\right]^T$ is a $K \times 1$ vector, and $\Phi^k = \text{diag}\left\{\xi_1^k, \xi_2^k, \ldots, \xi_K^k\right\}$ is a diagonal matrix of order K, we can derive that

$$\begin{aligned}
&\Omega_{1,m} \\
&= \begin{bmatrix} \psi_{1,m,1} & \psi_{1,m,1}\xi_1 & \cdots & \psi_{1,m,1}\xi_1^{K-1} \\ \psi_{1,m,2} & \psi_{1,m,2}\xi_2 & \cdots & \psi_{1,m,2}\xi_2^{K-1} \\ \vdots & \vdots & \ddots & \vdots \\ \psi_{1,m,K} & \psi_{1,m,K}\xi_K & \cdots & \psi_{1,m,K}\xi_K^{K-1} \end{bmatrix} \\
&= \begin{bmatrix} \psi_{1,m,1} & & & \\ & \psi_{1,m,2} & & \\ & & \ddots & \\ & & & \psi_{1,m,K} \end{bmatrix} \begin{bmatrix} 1 & \xi_1 & \cdots & \xi_1^{K-1} \\ 1 & \xi_2 & \cdots & \xi_2^{K-1} \\ \vdots & \vdots & \ddots & \vdots \\ 1 & \xi_K & \cdots & \xi_K^{K-1} \end{bmatrix} \\
&= \mathbf{DV}
\end{aligned} \tag{66}$$

where $\mathbf{D} = \text{diag}\{\psi_{1,m,1}, \psi_{1,m,2}, \ldots, \psi_{1,m,K}\}$ is a diagonal matrix whose diagonal entries are not zero, $\mathbf{V}$ is a square matrix with the Vandermonde structure. Therefore, $\mathbf{D}$, $\mathbf{V}$, and $\Omega_{1,m}$ are all full rank matrices.

$\mathbf{A}_0 \in \mathbb{C}^{(M-K+1)\times K}$ is the Vandermonde matrix consisting of the first $M-K+1$ rows of the array response matrix $\mathbf{A}$. When $M-K+1 > K$, the rank of $\mathbf{A}_0$ is K. Therefore, $\overline{\mathbf{R}}_{1,m} = \mathbf{A}_0\Omega_{1,m}$ is a full rank matrix, and $\overline{\mathbf{R}}_1 = \left[\overline{\mathbf{R}}_{1,1}, \ldots, \overline{\mathbf{R}}_{1,M}\right]$ can deal with K coherent signals.

APPENDIX B

We now prove that the estimated elevation and azimuth angles are automatically matched in our method. In practice, the reconstructed array response matrix $\hat{\mathbf{A}} = \left[\mathbf{a}(\hat{\phi}_{e_1}), \mathbf{a}(\hat{\phi}_{e_2}), \ldots, \mathbf{a}(\hat{\phi}_{e_K})\right]$ can be formed according to (13), where $\{\hat{\phi}_{e_1}, \hat{\phi}_{e_2}, \ldots, \hat{\phi}_{e_K}\}$ are estimated elevation angles by (51), $\{e_1, e_2, \ldots, e_K\}$ is an arbitrary arrangement of $\{1, 2, \ldots, K\}$. We assume that $1, 2, \ldots, K$ are the p_1th, p_2th, …, p_Kth elements in $\{e_1, e_2, \ldots, e_K\}$, respectively. $\mathbf{A}$ in (13) and $\hat{\mathbf{A}}$ are related as

$$\begin{aligned}
\hat{\mathbf{A}}\left[\mathbf{i}_{p_1}, \mathbf{i}_{p_2}, \ldots, \mathbf{i}_{p_K}\right] &= \mathbf{A}, \\
\hat{\mathbf{A}} &= \mathbf{A}\left[\mathbf{i}_{p_1}, \mathbf{i}_{p_2}, \ldots, \mathbf{i}_{p_K}\right]^T
\end{aligned} \tag{67}$$

where $\mathbf{i}_p$ is a column vector of all zeros except for the pth element which equals 1, and $\left[\mathbf{i}_{p_1}, \mathbf{i}_{p_2}, \ldots, \mathbf{i}_{p_K}\right]^T = \left[\mathbf{i}_{e_1}, \mathbf{i}_{e_2}, \ldots, \mathbf{i}_{e_K}\right]$. Denote $\left[\mathbf{i}_{e_1}, \mathbf{i}_{e_2}, \ldots, \mathbf{i}_{e_K}\right]$ by $\mathbf{E}$. Naturally, $\mathbf{E}^{-1} = \mathbf{E}^T$, and we have

$$\begin{aligned}
\hat{\mathbf{A}}^\dagger &= \{\mathbf{AE}\}^\dagger \\
&= \left\{\{\mathbf{AE}\}^H\{\mathbf{AE}\}\right\}^{-1}\{\mathbf{AE}\}^H \\
&= \mathbf{E}^T\{\mathbf{A}^H\mathbf{A}\}^{-1}\mathbf{E}\mathbf{E}^T\mathbf{A}^H \\
&= \mathbf{E}^T\mathbf{A}^\dagger.
\end{aligned} \tag{68}$$

Substitution of (68) into (56) yields

$$\begin{aligned}\hat{\mathbf{A}}^{\dagger}\hat{\mathbf{R}}'_{(1:M,:)} &= \mathbf{E}^T\Gamma_x\mathbf{R}_s\mathbf{A}^H = \hat{\mathbf{W}}_x,\\ \hat{\mathbf{A}}^{\dagger}\hat{\mathbf{R}}'_{(M+1:2M,:)} &= \mathbf{E}^T\Gamma_y\mathbf{R}_s\mathbf{A}^H = \hat{\mathbf{W}}_y.\end{aligned} \tag{69}$$

Let $\hat{\mathbf{w}}_{x,k}$ and $\hat{\mathbf{w}}_{y,k}$ are the kth rows in $\hat{\mathbf{W}}_x$ and $\hat{\mathbf{W}}_y$, respectively. Note that $\mathbf{E}^T = \left[\mathbf{i}_{e_1}, \mathbf{i}_{e_2}, \ldots, \mathbf{i}_{e_K}\right]^T$, then we have the following equation:

$$\tan\theta_{e_k}\ \hat{\mathbf{w}}_{x,k} = \hat{\mathbf{w}}_{y,k}, \quad k = 1, 2, \ldots, K. \tag{70}$$

We can see that the arrangement of the azimuth angles extracted from (70) also follows $\{e_1, e_2, \ldots, e_K\}$. Hence, the azimuth angles obtained from (57) are automatically matched with $\{\hat{\phi}_{e_1}, \hat{\phi}_{e_2}, \ldots, \hat{\phi}_{e_K}\}$ which are estimated by (51).

REFERENCES

[1] H. Krim and M. Viberg, "Two decades of array signal processing research: The parametric approach," *IEEE Signal Process. Mag.*, vol. 13, no. 4, pp. 67–94, Jul. 1996.
[2] P. Palanisamy, N. Kalyanasundaram, and P. M. Swetha, "Two-dimensional DOA estimation of coherent signals using acoustic vector sensor array," *Signal Process.*, vol. 92, no. 1, pp. 19–28, Jan. 2012.
[3] J. X. Zhang, M. G. Christensen, S. H. Jensen, and M. Moonen, "Joint DOA and multi-pitch estimation based on subspace techniques," *EURASIP J. Adv. Signal Process.*, vol. 2012, no. 1, pp. 1–11, 2012.
[4] H. Huang, J. Yang, H. Huang, Y. Song, and G. Gui, "Deep learning for super-resolution channel estimation and DOA estimation based massive MIMO system," *IEEE Trans. Veh. Technol.*, vol. 67, no. 9, pp. 8549–8560, Sep. 2018.
[5] Y. D. Zhang, M. G. Amin, and B. Himed, "Sparsity-based DOA estimation using co-prime arrays," in *Proc. IEEE Int. Conf. Acoust., Speech Signal Process.*, May 2013, pp. 3967–3971.
[6] J. Cao, J. Liu, J. Wang, and X. Lai, "Acoustic vector sensor: Reviews and future perspectives," *IET Signal Process.*, vol. 11, no. 1, pp. 1–9, 2016.
[7] R. O. Schmidt, "Multiple emitter location and signal parameter estimation," *IEEE Trans. Antennas Propag.*, vol. AP-34, no. 3, pp. 276–280, Mar. 1986.
[8] R. Roy and T. Kailath, "Esprit-estimation of signal parameters via rotational invariance techniques," *IEEE Trans. Acoust., Speech, Signal Process.*, vol. 37, no. 7, pp. 984–995, Jul. 1989.
[9] J. Tao, W. Chang, and W. Cui, "Vector field smoothing for DOA estimation of coherent underwater acoustic signals in presence of a reflecting boundary," *IEEE Sensors J.*, vol. 7, no. 8, pp. 1152–1158, Aug. 2007.
[10] J. He and Z. Liu, "Two-dimensional direction finding of acoustic sources by a vector sensor array using the propagator method," *Signal Process.*, vol. 88, no. 10, pp. 2492–2499, Oct. 2008.
[11] J. Zhang, X. Xu, Z. Chen, M. Bao, X.-P. Zhang, and J. Yang, "High-resolution DOA estimation algorithm for a single acoustic vector sensor at low SNR," *IEEE Trans. Signal Process.*, vol. 68, pp. 6142–6158, 2020.
[12] J. He and Z. Liu, "Computationally efficient underwater acoustic 2-D source localization with arbitrarily spaced vector hydrophones at unknown locations using the propagator method," *Multidimensional Syst. Signal Process.*, vol. 20, no. 3, pp. 285–296, Sep. 2009.
[13] A. Nehorai and E. Paldi, "Vector-sensor array processing for electromagnetic source localization," *IEEE Trans. Signal Process.*, vol. 42, no. 2, pp. 376–398, Feb. 1994.
[14] S. Miron, N. Le Bihan, and J. I. Mars, "Quaternion-MUSIC for vector-sensor array processing," *IEEE Trans. Signal Process.*, vol. 54, no. 4, pp. 1218–1229, Apr. 2006.
[15] X. Gong, Y. Xu, and Z. Liu, "Quaternion ESPRIT for direction finding with a polarization sentive array," in *Proc. 9th Int. Conf. Signal Process.*, Oct. 2008, pp. 378–381.
[16] Y. Li, J. Q. Zhang, B. Hu, H. Zhou, and X. Y. Zeng, "A novel 2-D quaternion ESPRIT for joint DOA and polarization estimation with crossed-dipole arrays," in *Proc. IEEE Int. Conf. Ind. Technol. (ICIT)*, Feb. 2013, pp. 1038–1043.
[17] H. Chen, W. Wang, and W. Liu, "Augmented quaternion ESPRIT-type DOA estimation with a crossed-dipole array," *IEEE Commun. Lett.*, vol. 24, no. 3, pp. 548–552, Mar. 2020.
[18] N. L. Bihan and J. Mars, "Singular value decomposition of quaternion matrices: A new tool for vector-sensor signal processing," *Signal Process.*, vol. 84, no. 7, pp. 1177–1199, Jul. 2004.
[19] J. Zhao and H. Tao, "Quaternion based joint DOA and polarization parameters estimation with stretched three-component electromagnetic vector sensor array," *J. Syst. Eng. Electron.*, vol. 28, no. 1, pp. 1–9, Feb. 2017.
[20] F. Zhao, J. Li, X. Jiang, and G. Wang, "Quaternion based arrival angles and polarization estimation with a cylindrically shaped conformal array," in *Proc. IEEE Int. Conf. Real-time Comput. Robot. (RCAR)*, Jul. 2017, pp. 483–487.
[21] M. Hawkes and A. Nehorai, "Acoustic vector-sensor correlations in ambient noise," *IEEE J. Ocean. Eng.*, vol. 26, no. 3, pp. 337–347, Jul. 2001.
[22] S. Marcos, A. Marsal, and M. Benidir, "The propagator method for source bearing estimation," *Signal Process.*, vol. 42, no. 2, pp. 121–138, 1995.
[23] G. Wang, J. Xin, N. Zheng, and A. Sano, "Computationally efficient subspace-based method for two-dimensional direction estimation with L-shaped array," *IEEE Trans. Signal Process.*, vol. 59, no. 7, pp. 3197–3212, Jul. 2011.
[24] S. Liu, L. Yang, Y. Xie, Y. Yin, and Q. Jiang, "2D DOA estimation for coherent signals with acoustic vector-sensor array," *Wireless Pers. Commun.*, vol. 95, no. 2, pp. 1285–1297, Jul. 2017.
[25] T. Ahmed, X. Zhang, and W. U. Hassan, "A higher-order propagator method for 2D-DOA estimation in massive MIMO systems," *IEEE Commun. Lett.*, vol. 24, no. 3, pp. 543–547, Mar. 2020.
[26] C. Xueqiang, G. Jincheng, W. Chenghua, Z. Xiaofei, and Y. Qiu, "Non-circular DOA estimation algorithm via propagator method and Euler transformation," in *Proc. 3rd IEEE Int. Conf. Comput. Commun. (ICCC)*, Dec. 2017, pp. 835–842.
[27] J. Xin and A. Sano, "Computationally efficient subspace-based method for direction-of-arrival estimation without eigendecomposition," *IEEE Trans. Signal Process.*, vol. 52, no. 4, pp. 876–893, Apr. 2004.
[28] N. Xi and L. Liping, "A computationally efficient subspace algorithm for 2-D DOA estimation with l-shaped array," *IEEE Signal Process. Lett.*, vol. 21, no. 8, pp. 971–974, Aug. 2014.
[29] N. Tayem, K. Majeed, and A. A. Hussain, "Two-dimensional DOA estimation using cross-correlation matrix with L-shaped array," *IEEE Antennas Wireless Propag. Lett.*, vol. 15, pp. 1077–1080, 2016.
[30] S. Kikuchi, H. Tsuji, and A. Sano, "Pair-matching method for estimating 2-D angle of arrival with a cross-correlation matrix," *IEEE Antennas Wireless Propag. Lett.*, vol. 5, no. 1, pp. 35–40, Dec. 2006.
[31] J.-F. Gu, P. Wei, and H.-M. Tai, "2-D direction-of-arrival estimation of coherent signals using cross-correlation matrix," *Signal Process.*, vol. 88, no. 1, pp. 75–85, Jan. 2008.
[32] J. He and Z. Liu, "Efficient underwater two-dimensional coherent source localization with linear vector-hydrophone array," *Signal Process.*, vol. 89, no. 9, pp. 1715–1722, Sep. 2009.
[33] R. J. Kozicka and S. A. Kassamb, "A unified approach to coherent source decorrelation by autocorrelation matrix smoothing," *Signal Process.*, vol. 45, no. 1, pp. 115–130, Jul. 1995.
[34] K. T. Wong and M. D. Zoltowski, "Closed-form underwater acoustic direction-finding with arbitrarily spaced vector hydrophones at unknown locations," *IEEE J. Ocean. Eng.*, vol. 22, no. 3, pp. 566–575, Jul. 1997.
[35] F. D. Neeser and J. L. Massey, "Proper complex random processes with applications to information theory," *IEEE Trans. Inf. Theory*, vol. 39, no. 4, pp. 1293–1302, Jul. 1993.
[36] P. J. Schreier and L. L. Scharf, "Second-order analysis of improper complex random vectors and processes," *IEEE Trans. Signal Process.*, vol. 51, no. 3, pp. 714–725, Mar. 2003.
[37] W. A. Kuperman and F. Ingenito, "Spatial correlation of surface generated noise in a stratified ocean," *J. Acoust. Soc. Amer.*, vol. 67, no. 6, pp. 1988–1996, 1980.
[38] R. J. Talham, "Noise correlation functions for anisotropic noise fields," *J. Acoust. Soc. Amer.*, vol. 35, no. 11, p. 1885, 1963.
[39] A. Nehorai and E. Paldi, "Acoustic vector-sensor array processing," *IEEE Trans. Signal Process.*, vol. 42, no. 9, pp. 2481–2491, Sep. 1994.
[40] S. U. Pillai and B. H. Kwon, "Forward/backward spatial smoothing techniques for coherent signal identification," *IEEE Trans. Acoust., Speech Signal Process.*, vol. 37, no. 1, pp. 8–15, Jan. 1989.

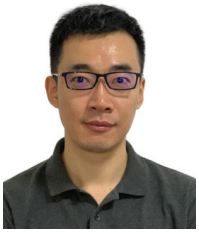

YI LOU received the B.Sc. degree in communication engineering from Jilin University, Jilin, China, in 2009, and the M.Sc. and Ph.D. degrees in information and communication engineering from the Harbin Institute of Technology, Harbin, China, in 2013 and 2017, respectively. He was a Visiting Student with The University of British Columbia, Kelowna, BC, Canada, in 2016. He is currently a Lecturer with the College of Underwater Acoustic Engineering, Harbin Engineering University, Harbin. His research interests include energy harvesting wireless communications, underwater communications, cooperative communications, and cognitive radio networks.

XINGHAO QU received the B.S. degree from Harbin Engineering University, Harbin, China, in 2021, where he is currently pursuing the Ph.D. degree in communication engineering. His research interests include array signal processing and source localization.

YINHENG LU (Graduate Student Member, IEEE) received the B.S. degree from Harbin Engineering University, Harbin, China, in 2018, where he is currently pursuing the Ph.D. degree in communication engineering. His research interests include in-band full duplex underwater acoustic communication and array signal processing.

GANG QIAO (Member, IEEE) received the B.S., M.S., and Ph.D. degrees in underwater acoustic engineering from Harbin Engineering University (HEU), Harbin, China, in 1996, 1999, and 2004, respectively. He visited the Department of Electrical Engineering, University of Washington, Seattle, WA, USA, as a Senior Visiting Scholar, in 2015. Since 2007, he has been a Full Professor with HEU. His research interests include underwater acoustic communication and networking, and underwater acoustic target detection and localization.